(2)

THERMOELECTRIC CONVERSION WITH ION CONDUCTORS

Final Report
Contract #N00014-86-C-0827

Submitted to
Office of Naval Research
800 North Quincy Street
Arlington, Virginia 22217-5000

Submitted by

Principal Investigator
Dr. Ashok V. Joshi

Ceramatec, Inc.
2425 South 900 West
Salt Lake City, Utah 84119

January, 1990

Ceramatec No. 90610/55001

TABLE OF CONTENTS

STATEMENT "A" per Dr. Robert Nowak
ONR, Code 1113
TELECON 2/7/90 CG

1.0 ABSTRACT:

A theoretical and experimental investigation of an oxygen thermoelectric generator based on oxygen ion-conducting solid electrolyte was carried out. In this thermoelectric generator concept, oxygen is electrochemically expanded at a higher temperature T and compressed at T_i ($T_i < T_h$). The purpose of this program was to establish the theoretical and experimental foundation necessary for assessment of feasibility of this concept for potential application to space power systems.

Several types of oxygen ion conducting solid electrolytes were successfully fabricated and electrochemically tested. Optimization of electrolyte/electrode couples improved performance and decreased degradation over time. A bi-element oxygen thermoelectric generator was designed, fabricated, and operated. Initially, the power derived was observed to be substantially lower than expected on the basis of earlier theoretical analysis. The maximum power realized through this heat engine was less than 20 $\mu W/cm^2$. In order to examine the source of the discrepancy, further theoretical analysis was conducted. The results of the analysis indicated that power exhibits a maximum as a function of the ratio of the partial pressures of oxygen in the two chambers (low and high pressure chambers). The power densities observed experimentally were in accord with this analysis. In view of this, a new concept of oxygen heat engine was devised in which the low pressure chamber contains a mixture of H_2O and H_2, both at sufficiently high levels. The H_2O/H_2 mixture ensures low O_2 pressure which allows high Nernst potential. At the same time, the transport of oxygen in the low pressure chamber occurs by the conversion and/or diffusion of H_2O, thereby essentially eliminating mass transport limitations. Observed power densities using this new concept were as high as 450 $\mu W/cm^2$, a significant improvement over the earlier thermoelectric generator trials. Theoretical analysis indicated that if the electrolyte and charge transfer resistances can be reduced, power densities in excess of 100 mW/cm^2 are possible. It should be recognized, however, that the analysis assumes no electrode losses. A substantial effort is still required towards the development of this device with appropriate electrode/electrolyte combinations to make this project commercially viable.

Key words: oxygen thermoelectric generator
- thermoelectric generator
oxygen solid electrolyte
space power (EMK)

2.0 TECHNICAL BACKROUND

Harwig and Gerards (1) have reported a high temperature form of bismuth oxide, which when stabilized in the face centered cubic phase, exhibits high oxygen ion conductivity in the range 500 C-600 C. The use of stabilized zirconia as a high temperature oxygen ion conducting membrane in a heat engine was patented by Ruka and Weissbart in 1968 (2). They conceived of a zirconia membrane fitted with suitable electrodes through which gaseous oxygen, the working fluid, was expanded isothermally at high temperature T2 and compressed at some lower temperature T1. They did not recommend the use of a stabilized zirconia membrane for the compressor, but instead suggested that the compressor might be "any of the well known mechanical devices for compressing gases". By developing a stable low temperature oxygen ion conductor, such as stabilized bismuth oxide, a thermoelectric generator can be devised using zirconia for the high temperature expander and bismuth oxide for the low temperature compressor.

Several unique features such as the absence of moving parts, low maintenance, compactness and modularity, high efficiency, and simplicity of the system make this concept attractive for space platform and satellite applications.

3.0 PROGRAM OBJECTIVES

The principal long range objectives of this three year program is to develop a working prototype of an oxygen heat engine (OHE) based on zirconium oxide for the oxygen expander and bismuth oxide as the oxygen compressor. The specific objectives of this program are:

1) Establish reliable methods for the fabrication of dense stabilized bismuth oxide solid electrolytes.

2) Explore techniques for the preparation of efficient electrodes for both solid electrolyte membranes in the OHE.

3) Measure D.C. voltage-current characteristics of candidate bismuth oxide and zirconium oxide electrolyte/electrode systems as a function of temperature and time.

4) Fabricate a model for the power capability and thermal conversion efficiency in sufficient detail for an assessment of potential device application to space power systems.

5) Construct a bi-element cell with appropriate electrolye/electrode couples to demonstrate the concept and identify any unforseen problems.

6) Pursue development of high temperature electrodes on zirconia for the high temperature cell.

7) Characterize the low temperature electrolyte in terms of strength and thermal expansion coefficient.

During the course of this work, the following questions were addressed.

1) Which are the appropriate solid electrolytes for the intended application?

2) What are the optimum conditions of temperature and applied voltage from the standpoint of electrolyte stability?

3) What are the realistic temperature limits from the standpoint of application?

4) What is the maximum theoretical power capability and thermal conversion efficiency?

5) Will the electrolyte/electrode systems have a reasonable life expectancy at temperatures and under the pertinent conditions of atmosphere?

4.0 PROJECT APPROACH

INTRODUCTION

The possibility of constructing practical electrochemical heat engines (often designated Thermally Regenerative Electrochemical Systems- TRES) has intrigued scientists for the past twenty-five years. A comprehensive review of these systems was prepared in 1980/1981 by H.L. Chum and R.A. Osteryoung (3) for SERI. They classified the various known systems into seven types. Type 7, which includes both the Sodium Heat Engine and the Oxygen Heat Engine is defined as follows:

"Type 7 engines are based on pressure differences of the working electroactive fluid across an isothermal electrolyte (solid or liquid). The pressure difference is maintained by using the

changes in the vapor pressure with the temperature of the working electroactive fluid. The work performed is equivalent to the isothermal expansion of the working electroactive fluid from the high to the low pressure zone at T2 through the electrolyte and its interfaces. After expansion, the working fluid is condensed in a cold reservoir and can be recycled to the high temperature, high pressure zone of the cell by means of a pump. The cells are concentration cells. Because the working fluid does not undergo chemical changes, no regeneration and separation steps are necessary. Examples include iodine vapor expanded through isothermal liquid lead iodide and sodium vapor expanded through isothermal sodium beta-alumina electrolyte. In the first example, the major difficulty is maintenance of the liquid electrolyte integrity when it is subjected to a pressure gradient. In the second example (T1 800 C-900 C), this problem is avoided by using a solid superionic conductor electrolyte. The highest outputs in TRES to date have been obtained with this type of engine. The present non-availability of other superioic conductors limits the extension of this concept to other practical energy converters."

OXYGEN HEAT ENGINE

A heat engine can be envisioned in which oxygen can be expanded through a zirconium oxide membrane at 1000 C-1200 C and then compressed at approximately 500 C-600 C, using a modified bismuth oxide membrane as a solid electrolyte. The net electrical work per unit charge in the limit of zero current (reversible process) is the difference between the work done by the system minus the work on the the system during compression.
This is given by

$$W=\frac{R\,(T_2-T_1)}{2}\,\ln\,(P_2/P_1)$$

and the corresponding conversion efficiency is simply given by

$$n=\frac{T_2-T_1}{T2}$$

which is the efficiency of a Carnot cycle.

This result is obtained by assuming that there is perfect heat exchange across the gas flow between the two reservoirs at differing temperatures. For the conditions cited above, a maximum theoretical efficiency of about 40% is possible. The actual efficiency under load will of course be less, perhaps on the order of 20%.

In the following pages, work performed during this three year project is described. Additionally, a theoretical analysis was undertaken to fully examine the capabilities of the proposed OHE. The pertinent theoretical analysis, its implications from the standpoint of the proposed OHE, and a modified OHE concept are also described in detail.

TASK 1.0 ELECTROLYTE/ELECTRODE DEVELOPMENT

The objective of this task was primarily to develop a low temperature electrolyte/electrode couple to be used for the compressor leg of the OHE. Aditionally, a high temperature electrode was to be developed for the zirconia membrane as the oxygen expander. Process development was to include formulation of oxygen conductive ceramic powders, fabrication of electrolyte membranes of tubular geometry, construction of oxygen conducting electrochemical cells, and characterization of the conduction properties of these cells under various conditions of temperature and atmosphere. The most promising cells, identified by the above characterization, were to be used later to demonstrate and evaluate a prototype oxygen thermoelectric generator.

Subtask 1.1: Fabrication of Electrolytes:

At the beginning of this project, stabilized bismuth oxide was selected as the candidate for the low temperature compressor leg of the OHE. This material is known to be a good oxygen ion conductor at fairly low temperatures (1,4,5,6). Various dopants were wet mixed with bismuth oxide using zirconia media and ethanol as the solvent. The slurries were subsequently dried and then calcined in air at the appropriate temperature. The calcined materials were additionally milled to effect particle size reduction and increase sinterability. Calcined powders were examined by x-ray diffraction. After confirmation that this material was the highly oxygen conductive face centered cubic phase (denoted δ-bismuth oxide), organic binders were added to enhance green formability. The powder was then dried, sieved, and finally isostatically pressed in a tubular configuration. These tubes were then hang-fired to the necessary temperatures to produce concentric, straight, and dense electrolyte membranes. Appropriate electrodes were applied to optimize the oxygen transport characteristics. The electrolyte/electrode interface is extremely important in determining the charge transfer characteristics of the cell which directly relates to oxygen conduction efficiency.

Subtask 1.2: Electrolyte/Electrode Performance Testing:

These first bismuth oxide based electrolyte materials degraded with time at temperatures below 700 C, due to the slow phase transformation from the highly conductive cubic phase (δ-bismuth oxide) to the lower oxygen conductivity rhombohedral phase (γ-bismuth oxide).[figure 1] The effect of this phase transformation was a decrease in current density over time. Much work was done to stabilize the highly conductive cubic phase at these lower temperatures. A proprietary composition, developed by Dr. Anil Virkar (Ceramatec Technical Advisory Board member)

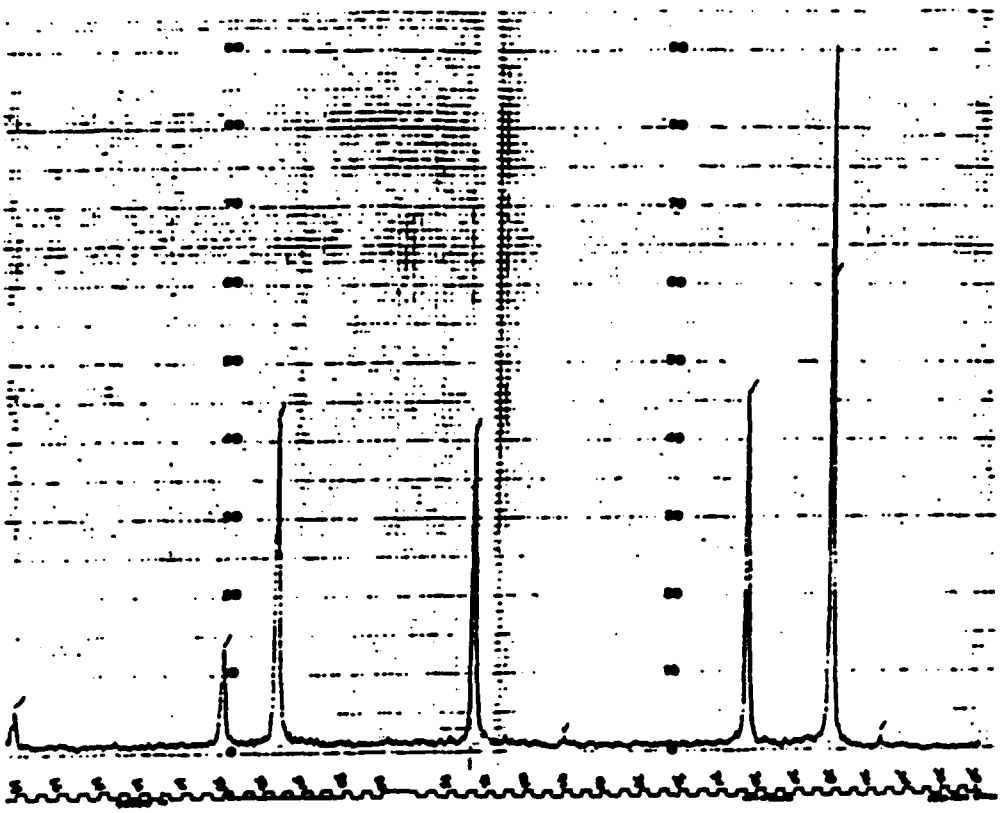

Before Testing

Figure 1 Peak splitting, an indication of δ to γ' phase change

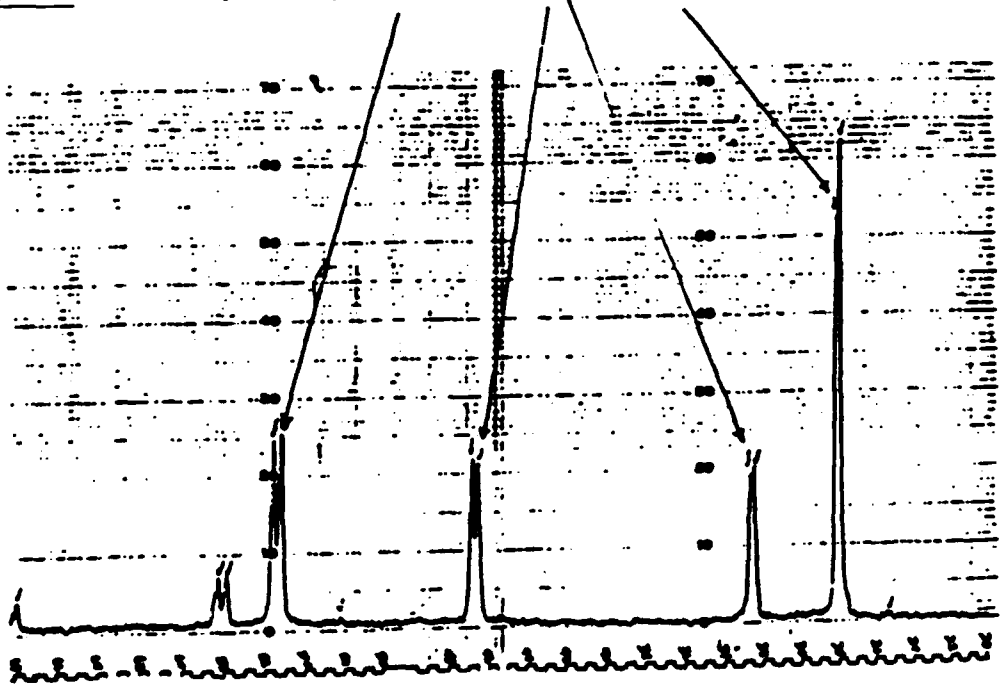

After Testing (800 hours)

and his graduate student at the University of Utah (on a program sponsored by the Gas Research Institute) did not exhibit this phase transformation after 1500 hours of testing.[figure 2] When a silver based electrode with silver wire as the current collector was tested on this bismuth oxide electrolyte, degradation was seen over a period of 1000 hours, due to both electrode and current collector detachment.

One major drawback to the bismuth oxide electrolyte material is its low strength. Addition of 10 wt% aluminum oxide to stabilized bismuth oxide increased the strength by approximately three times. Unfortunately, the aluminum oxide has a deleterious effect on the oxygen ion conductivity over time. In less than 100 hours the oxygen flow dropped by two orders of magnitude, due to both the reactivity between the aluminum oxide and the stabilizing dopant in the bismuth oxide, as well as the presence of the highly resistive aluminum oxide on the grain boundaries of the bismuth oxide.

All three of the electrolytes on which development was done showed material stability characteristics over time. Both zirconium oxide and cerium oxide, a material to be discussed in the next section, exhibit oxygen pumping characteristics which are stable for over 1000 hours, however bismuth oxide, in which the electrolyte itself showed promising phase stability, went through cell degradation during oxygen transport at temperatures below 700 C.

Development of high temperature electrolyte/electrode has moved in the direction of the elimination of silver as an electrode material. Problems with volatilization, related to the high mobility associated with operation so close to the melting point, limit the useful lifetime of a device. Cells with Lanthanum Strontium Manganite (LSM) as the base electrode and silver-palladium alloy overcoat with silver-palladium wire as current collector allow operation at higher temperatures. Cells have been operated at current densities between 110 and 125 mA/cm2 without any sign of degradation.[figure 3] In addition, LSM-platinum composite high temperature electrodes were developed and applied to a zirconia electrolyte which yielded a current density of 700 mA/ cm at 850 C.[figure 4]

Another avenue of development taken in the last year was the development of cerium oxide based electrolytes. The ionic conductivity of calcia-doped cerium oxide was about 100 times higher than that of stabilized zirconium oxide at 600 C (7,8,9), [figure 5]. The cerium oxide is doped in the cubic phase with the addition of calcium oxide, then processed similiarly to other electrolytes to produce dense, straight, closed-end tubes. Lanthanum Strontium Cobaltite (LSCo), a ceramic oxide-based electrode material with high electronic conductivity [figure 6], was prepared and applied to the stabilized cerium oxide tube. After firing the electrode on to form a good interface, a current collector was applied. The cell was then placed in a furnace and voltage applied to transport and collect oxygen for lifetime testing. Figures 7 and 8 show current density vs. temperature and

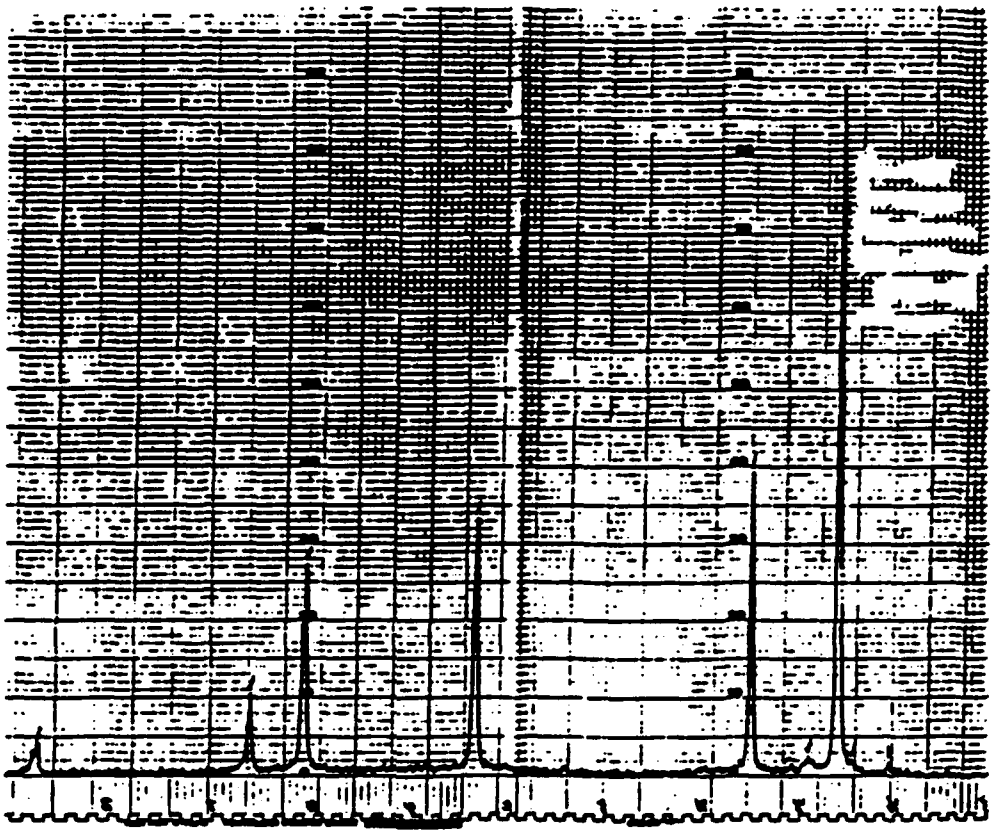

Before Testing

After Testing (1500 hours)

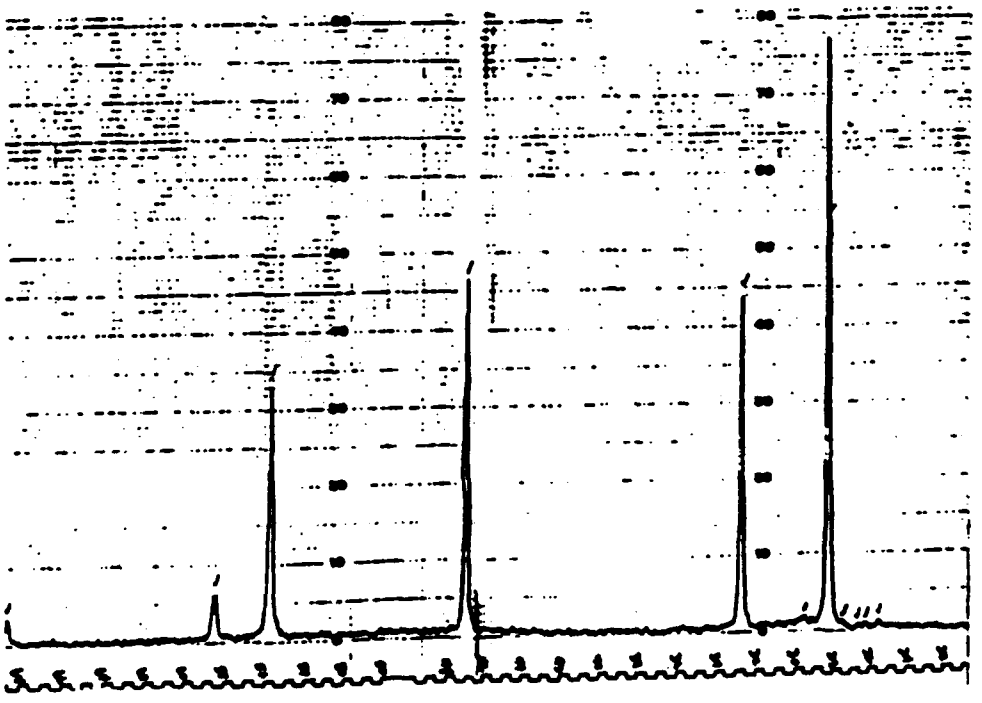

Figure 2 Note absence of peak splitting

Figure 3

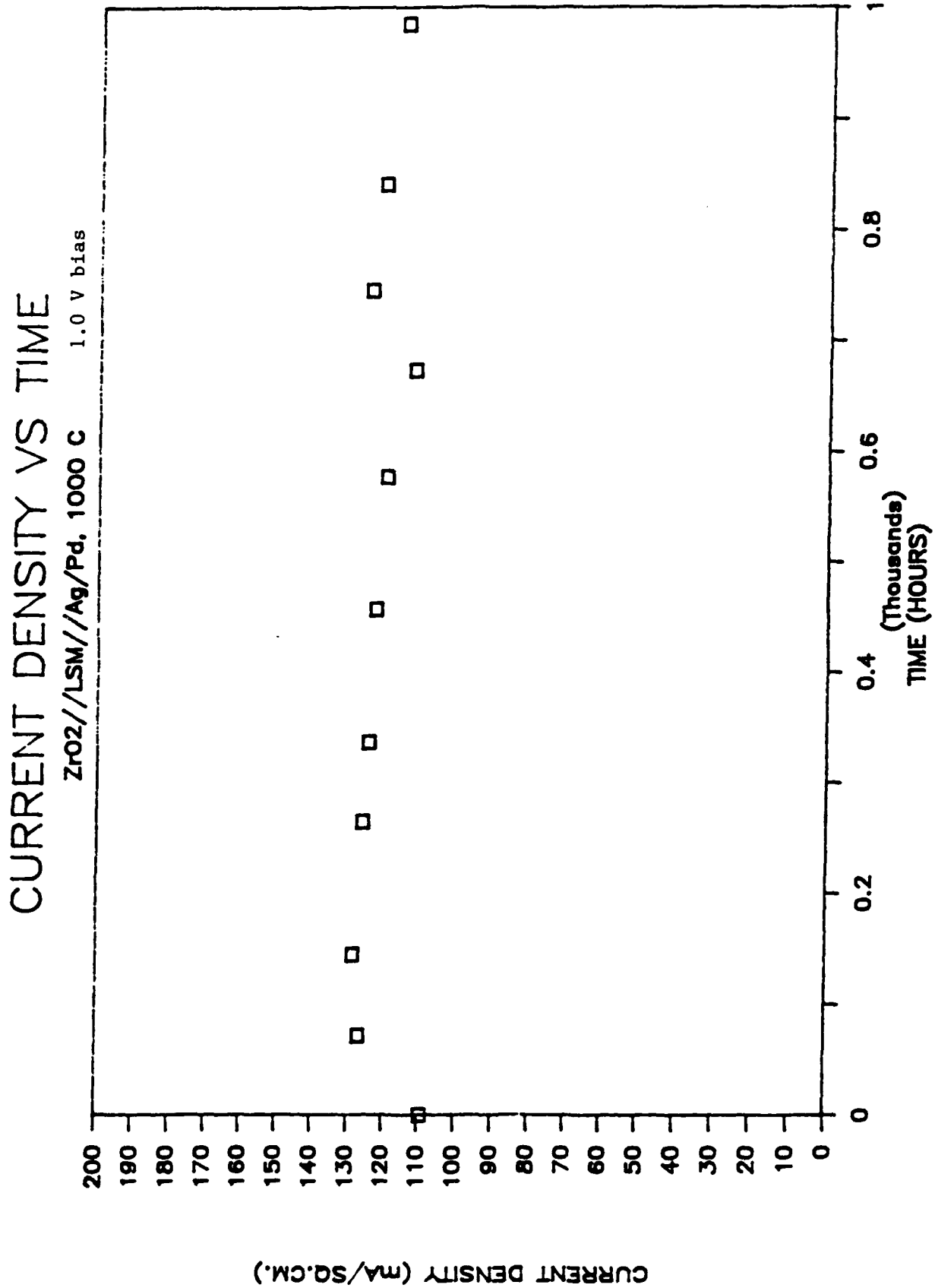
CURRENT DENSITY VS TIME
ZrO2//LSM//Ag/Pd, 1000 C
1.0 V bias
CURRENT DENSITY (mA/SQ.CM.)
200
190
180
170
160
150
140
130
120
110
100
90
80
70
60
50
40
30
20
10
0
0
0.2
0.4
0.6
0.8
1
TIME (HOURS)
(Thousands)

Figure 4

CURRENT DENSITY VS TEMPERATURE
Pt SPUTTER UNDER LSM
1.0 V bias, 850 C
CURRENT DENSITY (mA/SQ.CM.)
(Thousands)
1
0.9
0.8
0.7
0.6
0.5
0.4
0.3
0.2
0.1
0
0.7
0.74
0.78
0.82
0.86
0.9
0.94
0.98
TEMPERATURE (C)
(Thousands)

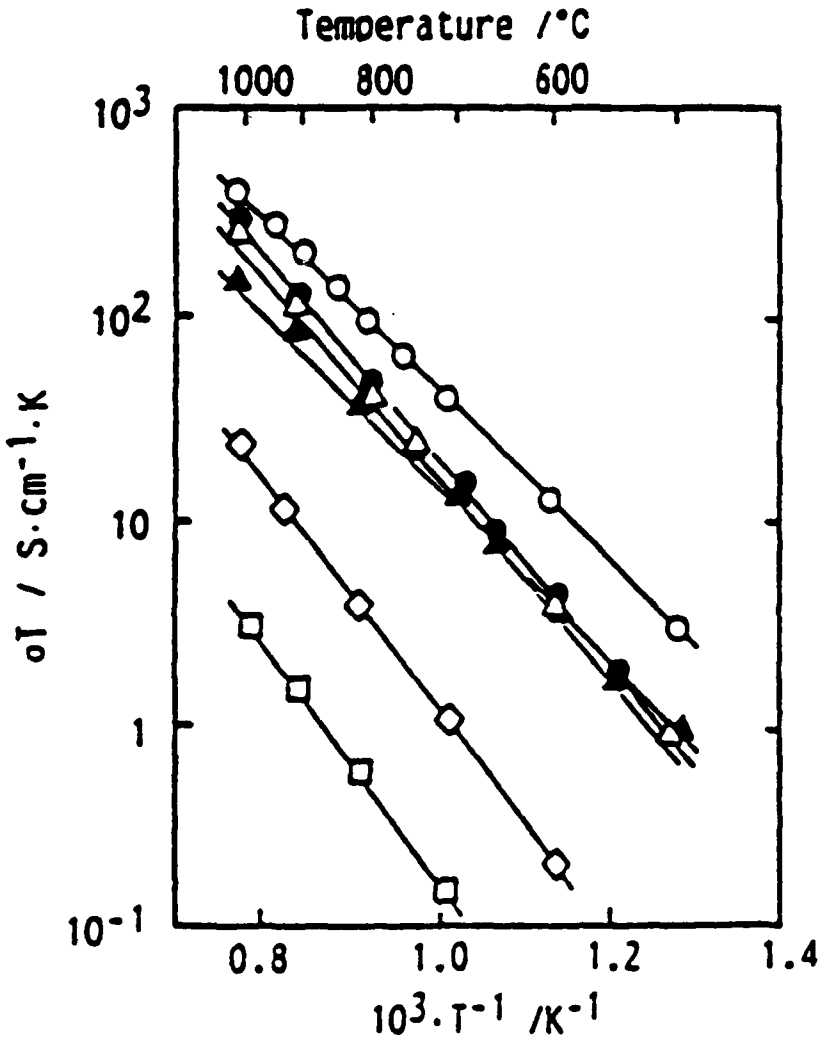

Fig. 5 Arrhenius plots for the electrical conductivities of $(\overline{CeO_2})_{0.8}(MO_{\nu})_{0.2}$, YSZ and CeO_2: M=(○)Sm, (△) Y, (●)Ca, (▲)Sr, (◇) $(ZrO_2)_{0.82}(YO_{1.5})_{0.18}$, (□)$CeO_2$.

Figure 6

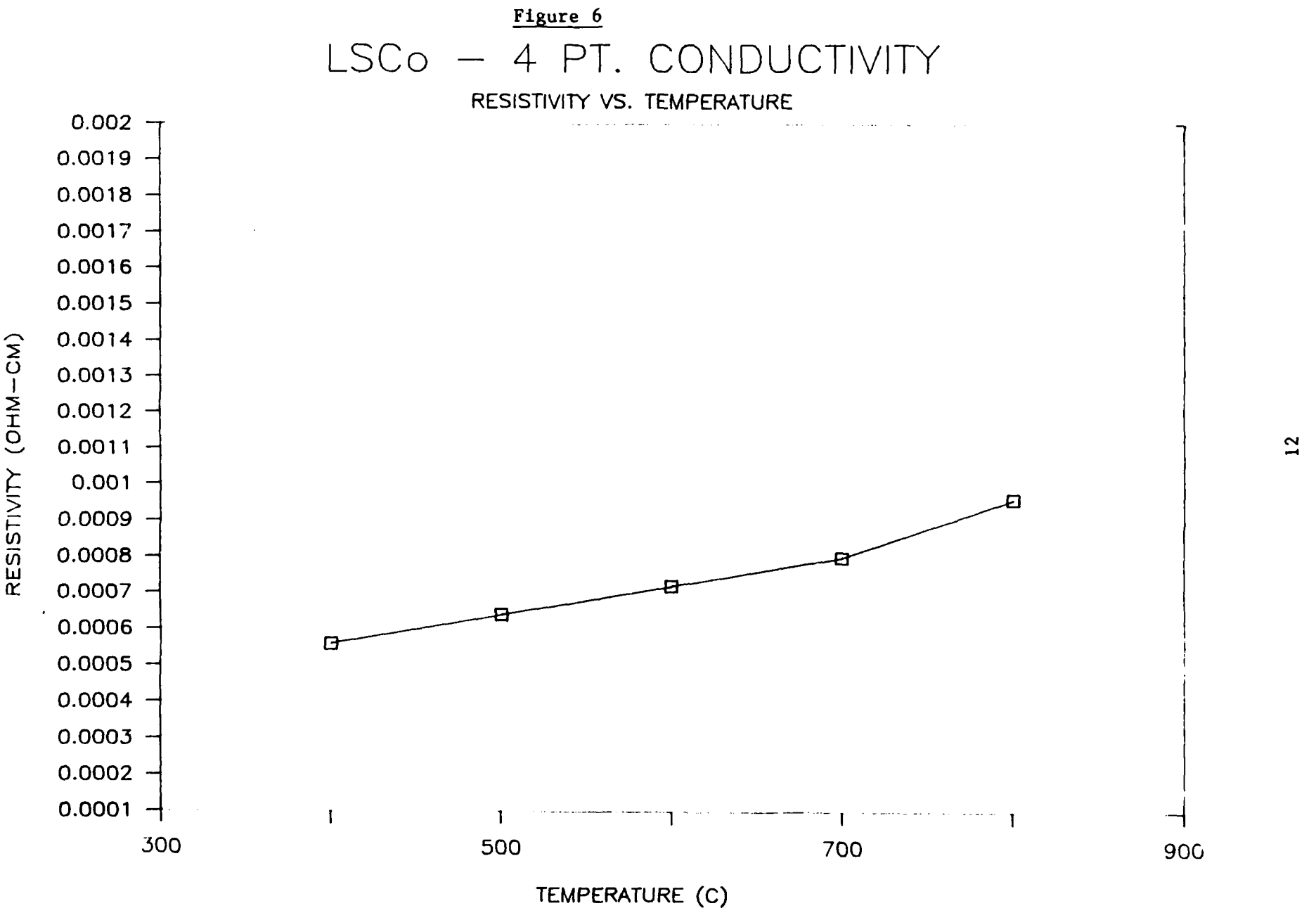
LSCo – 4 PT. CONDUCTIVITY
RESISTIVITY VS. TEMPERATURE
RESISTIVITY (OHM-CM)
0.002
0.0019
0.0018
0.0017
0.0016
0.0015
0.0014
0.0013
0.0012
0.0011
0.001
0.0009
0.0008
0.0007
0.0006
0.0005
0.0004
0.0003
0.0002
0.0001
300
500
700
900
TEMPERATURE (C)
12

Figure 7
CeO2-CaO w/ LSCo,Ag
current density vs. temperature
current density (mA/cm2)
450
400
350
300
250
200
150
100
50
0
500
540
580
620
660
700
740
780
temperature (C)
□ 0.2 V
+ 0.5 V
◇ 0.75 V
△ 1.0 V

Figure 8

CURRENT DENSITY VS TIME
CeO2 (15m/o CaO)//LaSrCoO3
0.5 V bias, 800 C
CURRENT DENSITY (mA/SQ.CM.)
TIME (HOURS)
(Thousands)
0
20
40
60
80
100
120
140
160
180
200
220
240
260
0
0.2
0.4
0.6
0.8
1
1.2
1.4

current density vs. time at 800 C respectively.

Significant results have shown quite high oxygen pumping efficiency compared to either zirconium oxide or bismuth oxide without any cell degradation caused by detrimental electrolyte phase change, uneven current density distribution causing microcracking, or electrode/current collector detachment. The use of this material will be mentioned later in the section on improved device operation concept.

TASK 2.0 TESTING AND EVALUATION OF A BI-ELEMENT THERMOELECTRIC DEVICE

The design for the optimization of a bi-element thermoelectric generator has been an ongoing development issue during the entire project. Our first design, used for the proof of concept, is shown in figure 9. This device produced less than 20 $\mu W/cm^2$ due to leakage problems in the test apparatus and electrode effects. The leakage was corrected by improving the laboratory scale apparatus with O-ring flange plates. The electrode property that was adversely affecting the power output of the device was nigh sheet resistance. We addressed that problem by increasing the thickness of the LSM electrode to improve current carrying capabilities of the cell. Although improvements were made that included reduced volume containment chambers, better seals, as well as material improvements which enhanced cell performance, power output was not significantly improved.

At this point we began to evaluate the operating parameters of the oxygen heat engine concept and came up with some limitations that may have caused the low power density achieved with earlier designs. In the existing designs, the high and low pressure cells were located too far apart from each other for optimum transport of oxygen molecules from one to the other. Several attempts were made to eliminate this mass transport problem by decreasing the path length required for oxygen molecules to travel. A device was constructed with open ended tubes so that a circulating pump could be installed in-line to aid in molecular oxygen transport [figure 10]. By inserting the circulating pump in the low oxygen partial pressure chamber, the power density of this device was significantly increased by ten times [figure 11]. Results show that by circulationg the lower oxygen partial pressure atmosphere, thus reducing the mass transport limitation of oxygen, higher device efficiency could be obtained. Another approach to the elimination of mass transport limitations was the construction of a concentric cell device which would reduce the mean free path mentioned in appendix A. This device was constructed in such a way as to contain the high temperature cell inside the low temperature cell. The low oxygen partial pressure chamber would be maintained between the interior of the low temperature cell and the exterior of the high temperature cell. The high pressure chamber was ambient air on the exterior of the low temperature cell and the interior of the high temperature cell. An internal heater was constructed and fitted into the high temperature cell. The entire assembly was placed into a furnace that was set for the temperature

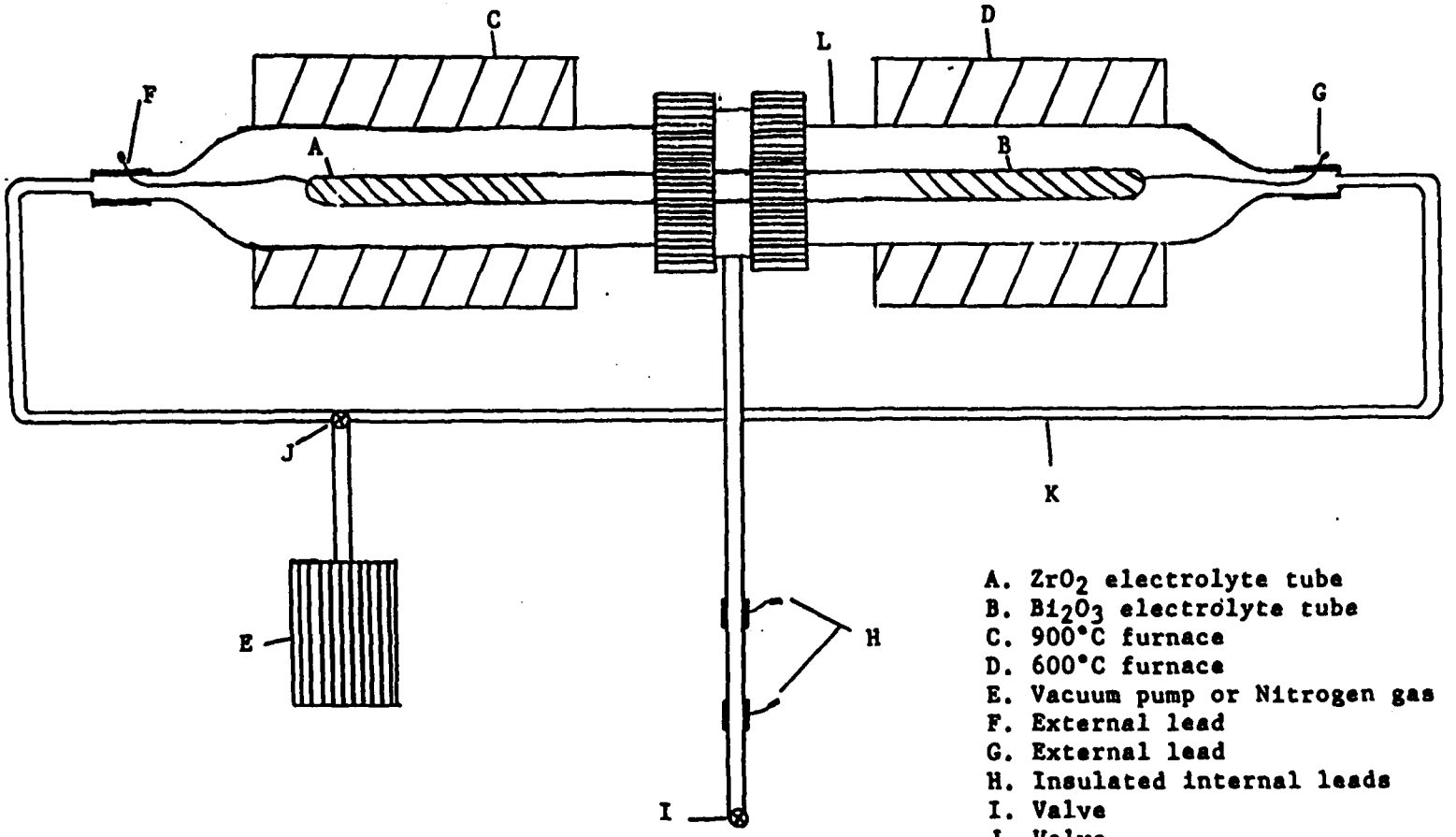

A. ZrO_2 electrolyte tube
B. Bi_2O_3 electrolyte tube
C. 900°C furnace
D. 600°C furnace
E. Vacuum pump or Nitrogen gas
F. External lead
G. External lead
H. Insulated internal leads
I. Valve
J. Valve
K. Bielement connecting tube
L. Quartz tube

Figure 9
Schematic diagram of experimental apparatus of Oxygen Thermoelectric Generator.

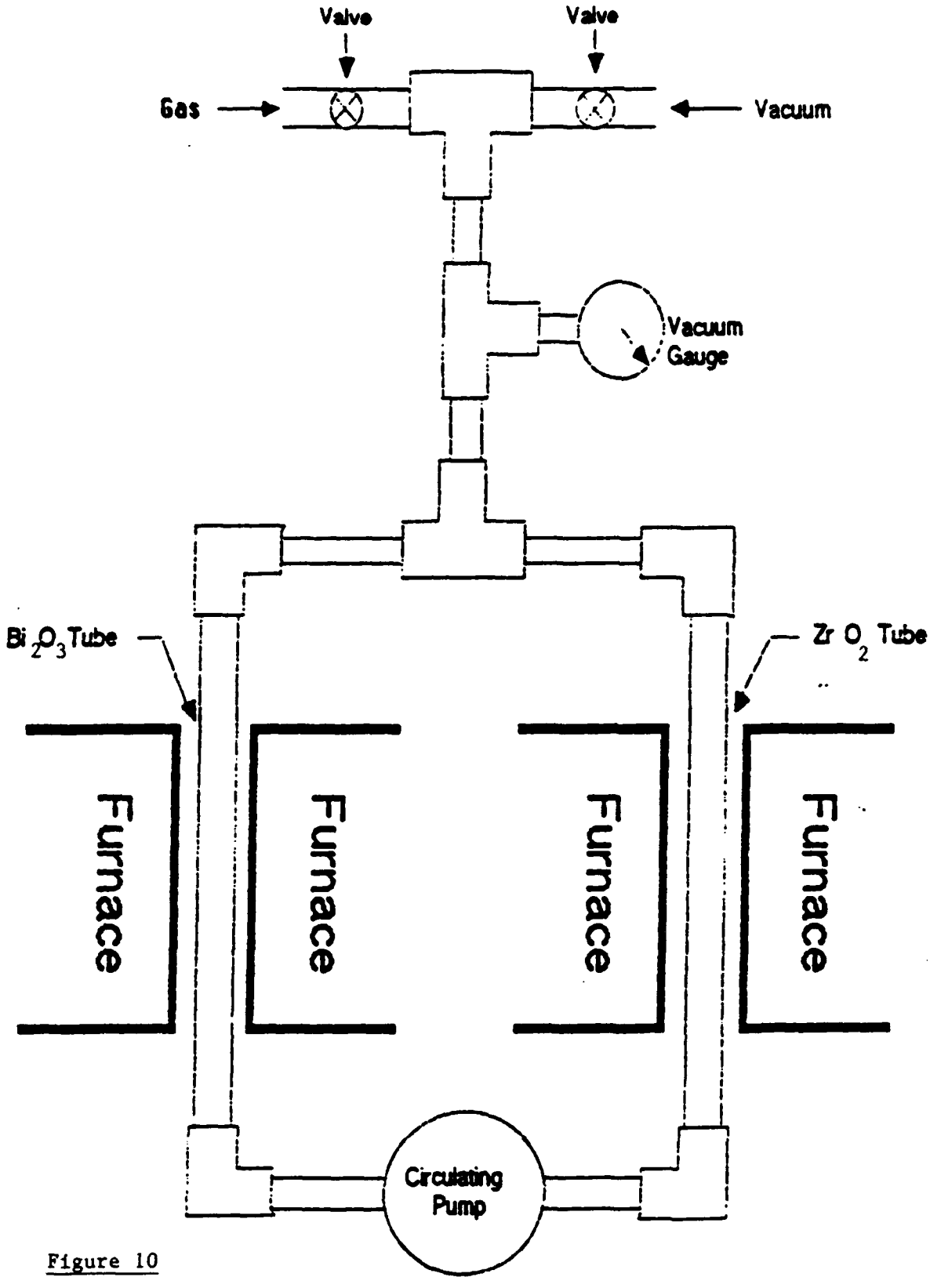
Valve
Valve
Gas
Vacuum
Vacuum
Gauge
Bi_2O_3 Tube
$Zr\ O_2$ Tube
Furnace
Furnace
Furnace
Furnace
Circulating
Pump

Figure 10

Figure 11

The Effect of Circulating Gases on Power Generation
(internal-10ppm O2/ external-air)

of the low temperature cell. Testing of this device was not successful due to sealing problems and the inability to maintain a sufficient temperature gradient between the two cells.

The best way to eliminate the mass transport limitation appeared to be by using a circulating pump in the low oxygen partial pressure chamber. We decided that this approach would be inconsistent with the final purpose of this device which is a high efficiency generator with no moving parts.

TASK 3.0 DEVELOPMENT OF IMPROVED DEVICE OPERATION CONCEPT

The final concept for elimination of mass transport limitation was a device referred to as the modified fuel cell concept found in appendix B. Devices were constructed to test this concept. A single stabilized zirconium oxide tube had two distinct electrode areas applied on the exterior, while only one continuous electrode was applied on the interior [figure 12].
These LSM electrodes were finally coated with silver-palladium paste and silver-palladium wire as current collectors.
Air was used on the exterior of the tube as the high oxygen partial pressure atmosphere for simplification. Hydrogen gas, bubbled through water, was introduced into the inside of the tube as the low oxygen partial pressure atmosphere. Figure 13 shows that the introduction of H_2/H_2O atmosphere to the low oxygen partial pressure chamber greatly increases power density relative to vacuum. When we put in sufficient insulation to increase the temperature gradient by 33% from 300 C to 420 C, the power output doubled again as seen in figure 14.

As mentioned in the section of electrolyte development , a material studied towards the end of the program was calcium oxide doped cerium oxide. Due to the promising transport characteristics and stability over time, this material was selected for fabrication of a single tube thermoelectric generator. The configuration was similiar to the single tube zirconium oxide device constructed previously. This electrolyte tube had successive LSCo electrodes applied in the same pattern as the previous zirconium oxide single cell experiment. Silver-palladium paste and silver-palladium wire were applied as the current collector to this single tube heat engine. Testing of this device was limited to a temperature differential of 200 C because of the length of this tube. Trials were run at 900 C vs. 700 C as well as 800 C vs. 600 C, both while running the low oxygen partial pressure chamber with either a vacuum or H_2/H_2O atmosphere. Results in figure 15 show that the heat engine run at 900 C/700 C produced four times the power density of the device run at 800 C/600 C, due to the increased conductivity of the electrolyte at elevated temperatures. This power density, the highest achieved in any OHE device so far, is approximately 450 $\mu W/cm^2$. The presence of H_2/H_2O significantly increased the power density over vacuum in the low oxygen partial pressure chamber, similiar to the effect on the single tube zirconium oxide device seen in figure 13. These experiments have shown that a reduction in the mass transport limitation by altering the device design greatly enhances the operating efficiency of an oxygen thermoelectric generator.

Figure 12

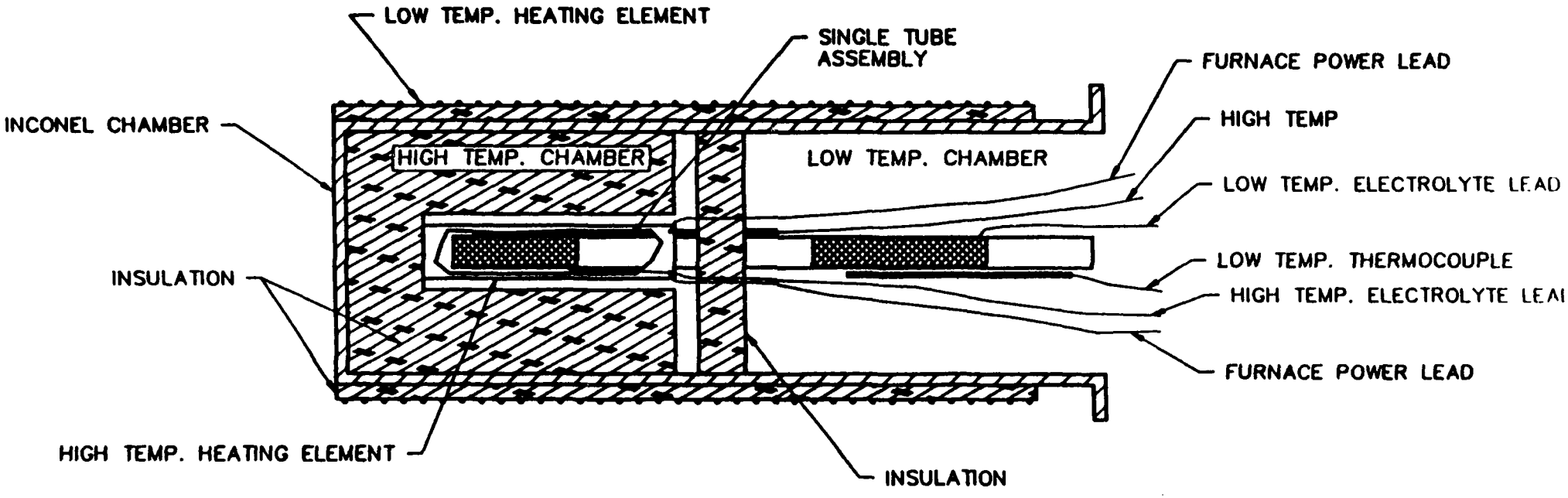

SCHEMATIC OF HIGH ΔT SINGLE TUBE
ELECTROCHEMICAL THERMOELECTRIC GENERATOR

Figure 13

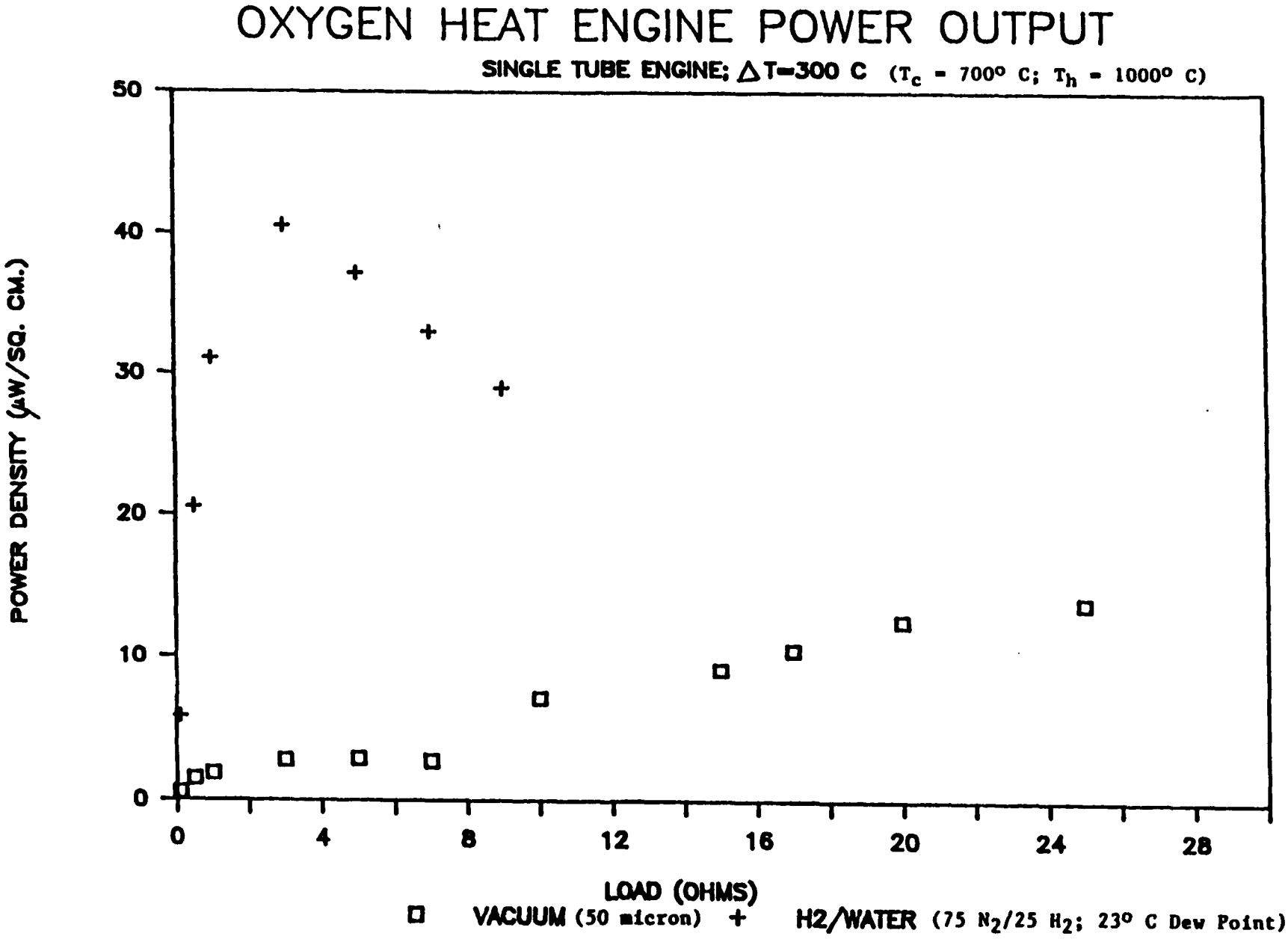
OXYGEN HEAT ENGINE POWER OUTPUT
SINGLE TUBE ENGINE; ΔT=300 C (T_c = 700° C; T_h = 1000° C)
POWER DENSITY (μW/SQ. CM.)
50
40
30
20
10
0
0
4
8
12
16
20
24
28
LOAD (OHMS)
VACUUM (50 micron)
H2/WATER (75 N_2/25 H_2; 23° C Dew Point)

Figure 14

OXYGEN HEAT ENGINE POWER OUTPUT

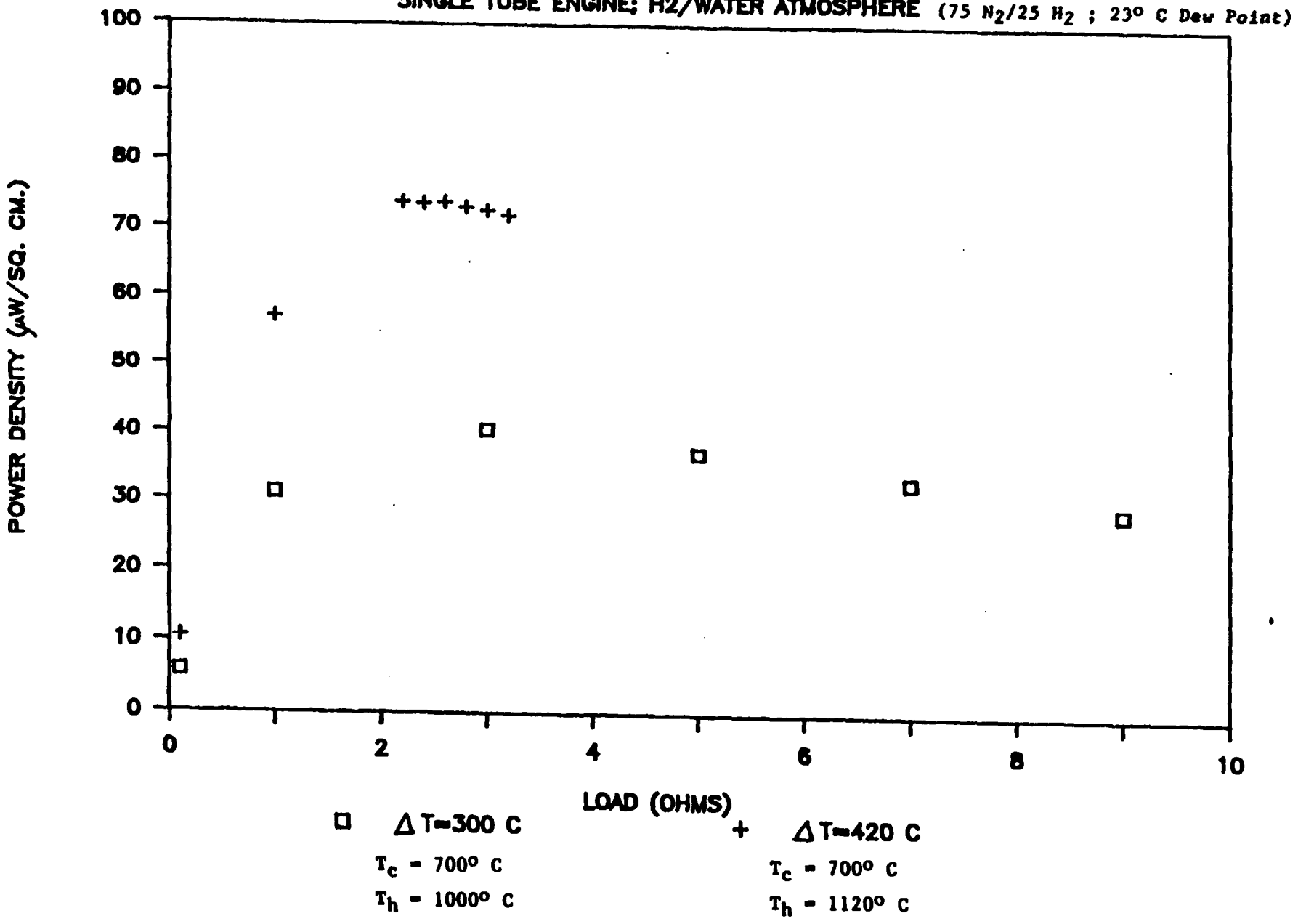

Figure 15

Cerium Oxide/LSCo Single Tube Heat Engine, Delta T=200C
(internal vacuum or H2/H20 vapor mix, external air)

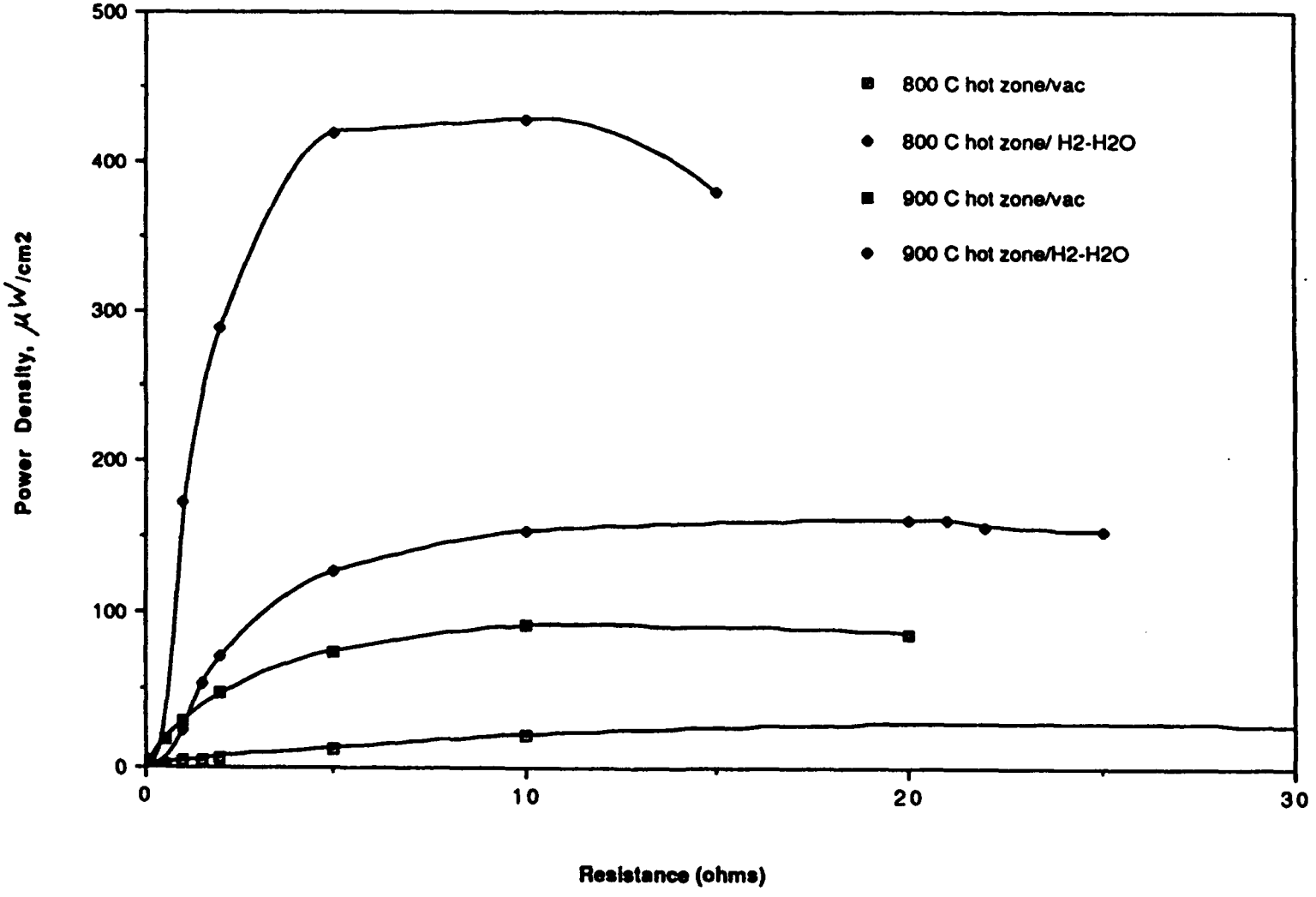

SUMMARY:

Oxygen ion conducting solid electrolytes were successfully fabricated and electrochemically tested. Zirconium oxide, Bismuth oxide, and Cerium oxide electrochemical cells were optimized for electrochemical oxygen transport. The power observed was substantially lower than expected on the basis of an earlier analysis. The reason for low power was traced to mass transport limitation in the low pressure chamber. In a new concept of the heat engine, the low presure chamber contains a mixture of H_2O and H_2, both at sufficiently high levels. The H_2O/H_2 mixture ensures low O_2 pressure which gives high Nernst potential. At the same time, the transport of oxygen in the low pressure chamber occurs by the convection and/or diffusion of H_2O, thereby essentially eliminating mass transport limitation.

APPENDIX A

OXYGEN HEAT ENGINE CALCULATIONS WITH MASS TRANSPORT LIMITATION IN THE LOW PRESSURE CHAMBER

Introduction:

The concept that has been proposed for an oxygen heat engine consists of an expansion of oxygen gas at high temperature (T_2) from pressure P_2 to P_1 followed by a compression at lower temperature (T_1) from P_1 to P_2 in a closed cycle. The proposed concept involves the use of zirconia electrolyte for expansion at T_2 and bismuth oxide for compression at T_1. The closed cycle concept in this two electrolyte design necessitates providing an electronic short between zirconia and bismuth oxide electrolytes in the low pressure chamber. As a result, the flux rate into (through zirconia) the low pressure chamber is exactly equal to the flux rate out (through bismuth oxide)of the low pressure chamber. This can place rather severe restrictions on the potential power that can be derived from such a device. It is important to recognize that this concept is radically different from the one used in the sodium heat engine in which the compression is achieved by simply recirculating liquid sodium and not by using another electrolyte. A schematic of the present heat engine concept is shown in Figure #1.

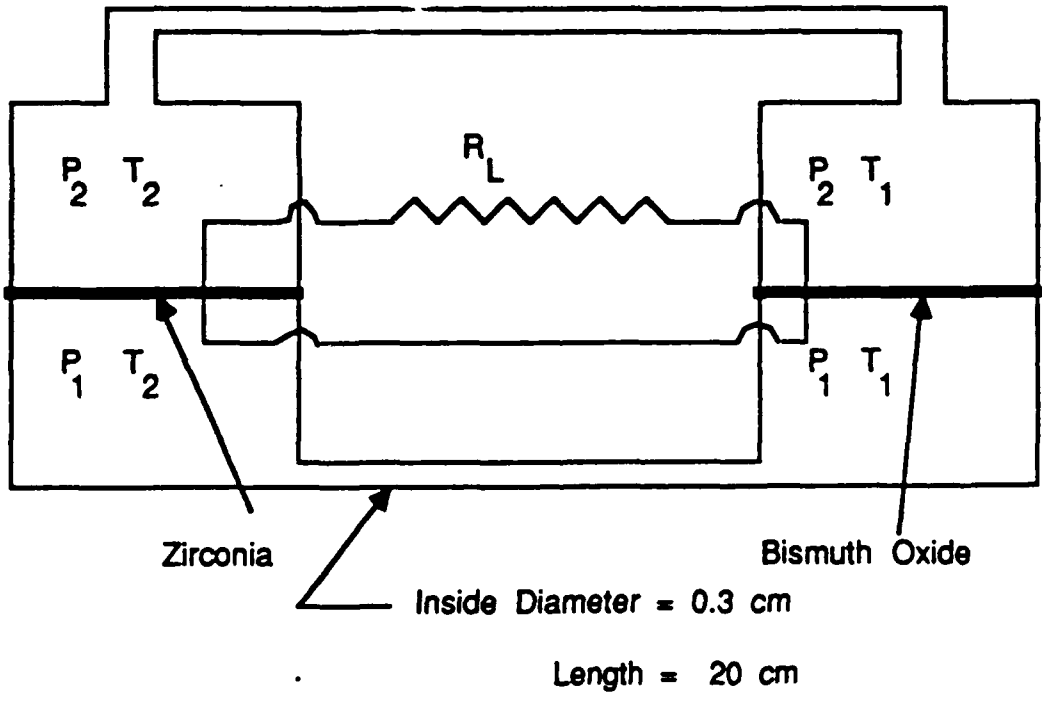

Figure #1: A schematic of the current heat engine design.

In what follows, calculations are presented assuming that the power achievable is limited by the

mass transport of oxygen in the low pressure chamber. It will be assumed that flux occurs by diffusion and that the pressure is sufficiently low such that the appropriate regime corresponds to the Knudsen regime. The diffusivity of a gas according to the kinetic theory of gases is given by

$$D = \frac{1}{3} v \langle \lambda \rangle \tag{1}$$

where v is the mean speed of gas molecules and $\langle \lambda \rangle$ is the mean free path. In what follows, estimates of $\langle \lambda \rangle$ and v are presented.

Mean Free Path:

From the kinetic theory of gases, we know that the mean free path, $\langle \lambda \rangle$, in a gas is given by

$$\langle \lambda \rangle = \frac{1}{\sqrt{2}\, n \sigma_o} \tag{2}$$

where n = number of molecules per unit volume and σ_o = molecular scattering cross section = $4\pi a^2$ where a is the molecular radius. At room temperature (300 K) and at an atmospheric pressure 9.65×10^5 dynes/cm^2, n is equal to 2.298×10^{19} /cm^3. Assuming d = 2 Å, the mean free path is determined to be $\langle \lambda \rangle \approx 2.45 \times 10^{-5}$cm = 2450 Å. Clearly, the mean free path increases with decreasing pressure. Table I gives the calculated values of $\langle \lambda \rangle$ at various pressures.

TABLE I

Pressure (atm)	Pressure (dynes/cm^2)	Mean Free Path, $\langle \lambda \rangle$, (cm)
1	9.65×10^5	2.45×10^{-5}
10^{-4}	96.5	0.245
10^{-5}	9.65	2.45
10^{-6}	0.965	24.5
10^{-7}	0.0965	245.0

Table I shows that for pressure $\leq 10^{-4}$ atm, the mean free path is comparable to the inside diameter of the tube that forms the low pressure chamber.

The Mean Speed of Gas Molecules:

According to the kinetic theory of gases, the mean speed is given by

$$v = \sqrt{\frac{2k_B T}{m}} \tag{3}$$

For oxygen, m = 32/(6.02 x 10^{23}) gm. At room temperature, the calculated value of v is 3.97 x 10^4 cm/sec. The diffusivity can now be determined using equation (1). However, for values of $\langle\lambda\rangle$ in excess of the smallest dimension of the low pressure chamber, e.g. the diameter of the tube d, the $\langle\lambda\rangle$ in equation (1) must be replaced by d. The diffusivity is then given by

$$D = \frac{1}{3}vd \tag{4}$$

If the inside diameter of the low pressure chamber is 0.3 cm, the corresponding diffusivity at room temperature is about 3.97 x 10^3 cm^2/sec. The diffusive flux of oxygen, J, is given by

$$J = -D\frac{dn}{dx} = -D\frac{d}{dx}\left(\frac{P}{k_B T}\right) = \frac{D}{k_B T}\frac{dP}{dx} \tag{5}$$

If the container size is much larger than the mean free pa$\ll \langle\lambda\rangle$ (which is not the case in the present design), which is given by

$$\langle\lambda\rangle = \frac{1}{\sqrt{2}n\sigma_o} = \frac{k_B T}{\sqrt{2}\sigma_o P} \tag{6}$$

the diffusivity is given by

$$D = \frac{1}{P\sigma_o}\sqrt{\frac{(k_B T)^3}{m}} \tag{7}$$

The corresponding flux is given by

$$J = -\frac{D}{k_B T}\frac{dP}{dx} = -\frac{1}{P\sigma_o}\sqrt{\frac{k_B T}{m}}\frac{dP}{dx} \tag{8}$$

Now, if the gradient in the pressure is proportional to the mean pressure itself, then the flux will be independent of the mean pressure. However, for $P \leq 10^{-4}$ atm, the mean free path is greater than the smallest dimension of the low pressure chamber. In such a case, the pertinent equation for diffusivity is equation (4) and not equation (7). In such a case, which corresponds to the current design, the flux is dependent upon the pressure within the low pressure chamber, provided the pressure gradient is proportional to the pressure itself.

A schematic of the pressure distribution in steady state with external resistor, R_L, in series is shown in Figure #2. When there is no external resistor in series (i.e. $R_L = \infty$), the pressure is uniform in the low pressure chamber. However, assuming mass transport limitation, when the external resistor is finite, there exists a pressure gradient in the low pressure chamber. In such a case, as shown in Figure #2, $P_a > P_1$ and $P_b < P_1$.

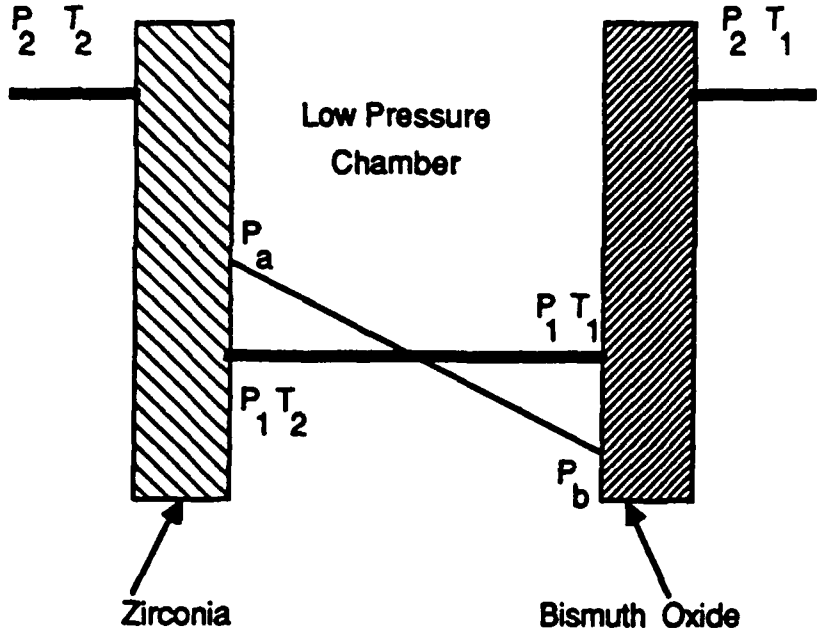

Figure #2: A schematic showing pressure distribution in the low pressure chamber when $R_L = \infty$ (thick line) and when R_L is finite (thin line).

The corresponding equivalent circuit is given in Figure #3.

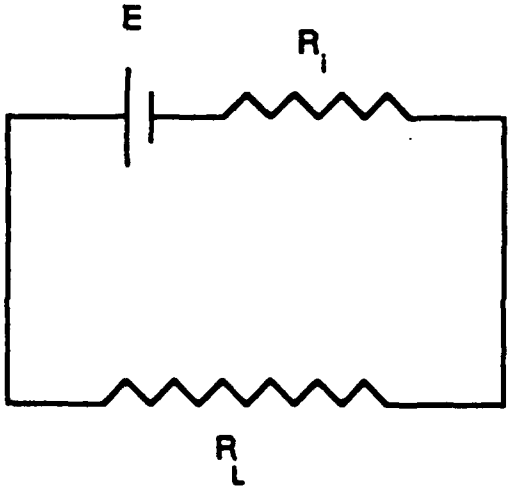

Figure #3: A schematic showing the equivalent circuit. R_i is the internal resistance of the heat engine. It will be assumed here that it is primarily due to the solid electrolytes. In reality, there may be a significant contribution from the electrodes.

In the case of conventional battery calculations, maximum power is realized when the external

resistance, R_L, which is the load, is equal to the internal resistance, R_i. As will be shown in the following, this is not the case when there is a mass transport limitation. When R_L is finite, in steady state, the pressure P_a and P_b are given by

$$P_a = P_1 + \frac{\Delta P}{2} \quad \text{and} \quad P_b = P_1 - \frac{\Delta P}{2} \tag{9}$$

In steady state the pressures are given in this manner since the mean pressure in the low pressure must be unaltered as the total number of moles are constant. However, this is true only if the temperature is constant in the low pressure chamber which is not the case. In the following calculations we will assume the temperature to be uniform at $T = (T_1 + T_2)/2$ for the sake of simplicity. Let us further write $\Delta P = 2\alpha P_1$. Then $P_a = (1+\alpha)P_1$ and $P_b = (1-\alpha)P_1$. The emf of the device is given by

$$E = E_2 - E_1 = \frac{RT_2}{4F} \ln\left(\frac{P_2}{P_a}\right) - \frac{RT_1}{4F} \ln\left(\frac{P_2}{P_b}\right) \tag{10}$$

Upon substituting for P_a and P_b in terms of P_1 and α, the emf is given by

$$E = \frac{R(T_2 - T_1)}{4F} \ln\left(\frac{P_2}{P_1}\right) - \frac{R}{4F}\left\{T_2 \ln(1+\alpha) - T_1 \ln(1-\alpha)\right\} \tag{11}$$

or

$$E = E_o - E(\alpha) \tag{12}$$

where E_o is the Nernst potential (open circuit potential) and $E(\alpha)$ is the correction term due to mass transport limitation in the low pressure chamber.

Evaluation of the Current in Terms of the Diffusive Flux:

The diffusive flux in the low pressure chamber is given by equation (5). The pressure gardient is given by

$$\frac{dP}{dx} = \frac{P_b - P_a}{L} = \frac{(1-\alpha)P_1 - (1+\alpha)P_1}{L} = -\frac{2\alpha P_1}{L} \tag{13}$$

where L is the length of the low pressure chamber. The flux of oxygen is thus given as

$$J = \frac{2D\alpha P_1}{k_B T L} \tag{14}$$

As there can be no continual buildup of charge, the current density is related to the flux via

$$I = \frac{4FJ}{N_o L} = \frac{8FD\alpha P_1}{RTL} = \frac{8eD\alpha P_1}{k_B TL} \qquad (15)$$

where N_o is the Avogadro's number and e is the electronic charge. In terms of the emf E and the total resistance of the circuit, which the sum of the internal and the external (load) resistances, the current density is also given by

$$I = \frac{E}{R_i + R_L} = \frac{R(T_2 - T_1)}{4F(R_i + R_L)} \ln\left(\frac{P_2}{P_1}\right) - \frac{R}{4F(R_i + R_L)} \left\{T_2 \ln(1+\alpha) - T_1 \ln(1-\alpha)\right\} \qquad (16)$$

Equating equations (15) and (16) gives an equation for α. This implicit equation is given as

$$\alpha = \frac{R^2 TL}{32F^2 DP_1(R_i + R_L)} \left[(T_2 - T_1) \ln\left(\frac{P_2}{P_1}\right) - \left\{T_2 \ln(1+\alpha) - T_1 \ln(1-\alpha)\right\}\right] \qquad (17)$$

The pertinent value of α can be obtained by solving the implicit equation by iteration. As mentioned earlier, for the sake of simplicity, the temperature T in the low pressure chamber is taken as the average of T_1 and T_2, i.e. $T = (T_1 + T_2)/2$. Also in the preceding analysis, R_i and R_L are specific ressistances in Ω-cm^2.

Calculations:

In the following, results of the calculations performed are given. The various data assumed for the calculations are given below:

ρ_z (zirconia) at 1000°C = 10 Ω-cm, ρ_b (bismuth oxide) at 700°C = 10 Ω-cm.

The wall thicknesses of both zirconia and bismuth oxide tubes are assumed to be 0.1 cm. The specific internal resistances of zirconia and bismuth oxide thus are $R_z = \rho_z$. thickness/unit area and $R_b = \rho_b$. thickness/unit area. Thus, $R_z = R_b = 1\ \Omega$-cm^2. The total internal resistance, R_i, is then given by $R_i = R_z + R_b = 2\ \Omega$-cm^2. In the calculations, the load, R_L, is chosen to be equal to the internal resistance. Hence, $R_i + R_L = 4\ \Omega$-cm^2.

It can verified that the units of α are erg.sec/Ω if we use the c.g.s system of units.
R, the gas constant = 1.987 cal/deg.mole = 8.3136×10^7 ergs/deg.mole.

Calculation of the diffusion coefficient: Assume $\langle\lambda\rangle = 0.3$ cm, the diameter of the low pressure chamber. Let $T_2 = 1273$ K (1000°C) and $T_1 = 973$ K (700°C). The mean speed (given by equation

(3)) for the average temperature $T = (T_1 + T_2)/2 = 1123$ K is given as $v = 7.68 \times 10^4$ cm/sec. The corresponding D via equation (4) is given by $D = 7.68 \times 10^3$ cm^2/sec.

The pressure,P_2, in the high pressure chamber is assumed to be 1 atm = 9.65×10^5 dynes/cm^2. The pressure, P_1, in the low pressure chamber was varied between 10^{-7} atm (0.0965 dynes/cm^2) and 10^{-4} atm (96.5 dynes/cm^2). Finally, the length of the low pressure chamber was assumed to be 20 cm. For the various values of P_1, equation (17) was solved by iteration in order to determine α. Once α was determined, the emf of the heat engine was determined and the corresponding power, given by E^2/R_L per sq. cm. was determined. Table II gives the results of these calculations.

TABLE II

Calculations of α, E and power for $\langle\lambda\rangle = 0.3$ cm.

P_2 (atm)	P_1 (atm)	α	E_o (mV)	$E(\alpha)$ (mV)	$E = E_o - E(\alpha)$ (mV)	Power = $E^2R_L/(R_i+R_L)^2$ (mW/cm^2)
1	10^{-3}*	0.042545	44.64	2.05	42.59	0.113
1	10^{-4}	0.0467855	59.52	2.26	57.26	0.41
1	5×10^{-5}	0.096423	64.00	4.65	59.35	0.44
1	10^{-5}	0.43	74.00	21.60	52.40	0.343
1	5×10^{-6}	0.674	78.88	41.26	37.62	0.177
1	10^{-6}	0.9417	89.3	69.8	19.5	0.0475
1	10^{-7}	0.982	104.10	102.95	1.15	0.00017

* For $P_1 = 10^{-3}$ atm, the mean free path used for the calculation of D is $\langle\lambda\rangle = 0.0245$ cm.

Similar calculations were made with the internal diameter of the low pressure chamber being 3 cm. The results of these calculations are given in Table III.

The preceding calculations show that if the pressure in the low pressure chamber is decreased indefinitely, power actually decreases and does not increase. For very low values of pressure in the low pressure chamber, the Nernstian potential, E_o, is high as expected. However, the relative value of the correction term, $E(\alpha)$, also increases drastically. As a result the net emf available for deriving power actually decreases. For example, as shown in Table II, for $P_1 = 10^{-7}$ atm, the E_o is 104.10 mV. However, the corresponding $E(\alpha)$ is 102.95 mV. Thus, the actual emf available is only 1.15 mV. The net result is that there is hardly any power. (Figure #4 shows a plot of power

TABLE III

Calculations of α, E and power for $\langle\lambda\rangle$ = 3 cm.

P_2 (atm)	P_1 (atm)	α	E_o (mV)	$E(\alpha)$ (mV)	$E = E_o - E(\alpha)$ (mV)	Power = $E^2/(R_i+R_L)^2$ (mW/cm^2)
1	10^{-5}	0.05848	74.40	2.80	71.60	0.64
1	10^{-6}	0.5133	89.30	26.50	62.80	0.49
1	10^{-7}	0.97027	104.10	92.30	11.90	0.0175

density vs. Log(P_1)). If there were no mass transport limitation, as assumed in the calculations reported previously, the power would have increased with decreasing P_1. According to the calculations presented here, it appears that inclusion of mass transport limitation is necessary, assuming that Knudsen flow is the dominant flow mechanism in the low pressure chamber.

The preceding calculations show that the the maximum power generated is only 0.64 mW/sq.cm. for the conditions chosen here. These conditions closely resemble the design of the current heat engine. Significant improvement in the power generated is possible if one minimizes L, the length of the low pressure chamber and increases the diameter. This may be achieved by a concentric tube design where a zirconia tube (heated to T_2 using an internal electrical heater) is placed inside a bismuth oxide tube at T_1. With such a design, it is possible to get somewhat higher power densities. However, when one recognizes that there would likely be substantial losses in the electrodes themselves (electrode/electrolyte interfaces as well as the flow of oxygen through porous electrodes), which have been neglected in the preceding calculations, the power densities generated would be reduced.

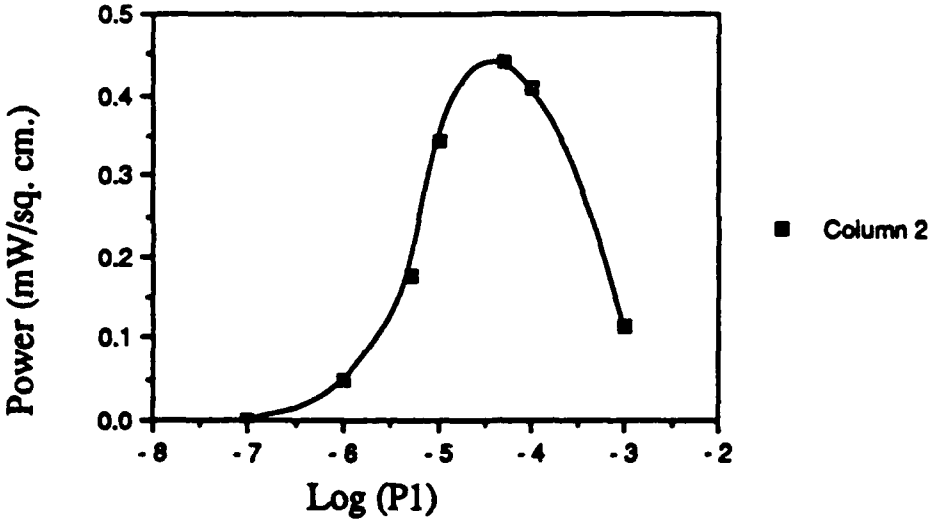

Figure #4: Calculated power density vs. Log(P_1).

APPENDIX B

A MODIFIED OXYGEN HEAT ENGINE:

As discussed in the preceding, in order to achieve high power it is necessary to ensure that the Nernst potential is high and that there is no mass transport limitation in the low activity chamber. Mass transport limitation leads to the correction term $E(\alpha)$ which subtracts out of the the Nernst potential E_o. This is clearly undesirable. With respect to equation (17), the implication is that the pressure (of oxygen) in the low pressure chamber must be high to ensure that mass transport limitation does not occur. These two requirements appear contradictory. However, both of these objectives can be met provided much of the oxygen in the low pressure chamber is tied up in some compound. In such a case, there is no mass transport limitation. At the same time as the partial pressure of oxygen is rather low, the Nernst potential will be high. This may be achieved by using a mixture of H_2O and H_2 in the low oxygen activity chamber. Both H_2O and H_2 are to be at sufficiently high partial pressures to prevent mass transport limitation. Also, at the same time this ensures high Nernst potential. This concept is described in what follows:

(B1): An $O_2/H_2O/H_2$ Heat Engine without Mass Transport Limitation: The calculations given in Section II show that there are two counteracting factors which limit the maximum achievable power. If the pressure in the low pressure chamber is decreased, the Nernst potential increases which should increase the power density. However, as the pressure is lowered, the current is lowered due to the mass transport limitation. For achieving high power density, both the current and the voltage achievable must be high. This can be achieved if the species responsible for current in the low pressure chamber is not the same as that is responsible for the Nernst potential. If this can be achieved, high power densities can be realized. A modified concept is proposed in what follows. Figure #B1 shows a schematic of such a design.

The low O_2-pressure chamber consists of a mixture of H_2O and H_2 gases, both at sufficiently high pressures.Thus, very low pressures of O_2 can be maintained in the low O_2-pressure chamber. This gives high enough Nernst potentials. At the same time the problem of mass transport limitation is circumvented as will be discussed in what follows. In this design, even in the absence of an external load, the partial pressure of oxygen in the low pressure chamber is not uniform. Actually, the pO_2^* and pO_2^{**} at the two electrolytes will be different and will be

dictated by the H_2O/H_2 equilibria at the respective temperatures. As the decomposition of H_2O into H_2 and O_2 is an endothermic process, the $pO_2^{**} > pO_2^{*}$ as $T_2 > T_1$.

In the low O_2-pressure chamber, the following reactions occur at the electrolyte surfaces.

<u>At T_2:</u> $H_2O(g) \rightarrow H_2(g) + 1/2\ O_2(g)$ An endothermic process.

$1/2\ O_2(g) + 2e' \rightarrow O^{-2}$

O^{-2} transports through the electrolyte to the high O_2-pressure chamber and the electrons transport through the outer circiut. In the high pressure chamber,

$$O^{-2} \rightarrow 1/2\ O_2(g) + 2e'$$

<u>At T_1:</u> $1/2\ O_2(g) + 2e' \rightarrow O^{-2}$ in the high O_2-pressure chamber.

O^{-2} transports through the electrolyte into the low O_2-pressure chamber. 2e' transport through the outer circuit. In the low pO_2-chamber

$$O^{-2} \rightarrow 1/2\ O_2(g) + 2e'$$

$$H_2(g) + 1/2O_2(g) \rightarrow H_2O(g) \qquad \text{An exothermic process.}$$

An important feature of this design is that Nernst potentials are governed by the ratios of partial pressures of O_2 in the high and the low pressure chambers at the two temperatures. By selecting appropriate pH_2O/pH_2 ratios, pO_2^{*} and pO_2^{**} can made be sufficiently small in order to generate high Nernst potentials. The current, on the other hand, is not dictated by the partial pressures of O_2 in the low pressure chamber; rather it is controlled by the rate at which H_2O and H_2 can be transported between the two electrolytes. As the partial pressures of both of these species is considerably greater than that of O_2, no mass transport limitation is expected.

In what follows, calculations are presented on the determination of the partial pressures of O_2 in the low pressure chamber for various values of pH_2O/pH_2 in the low pressure chamber and the emf's generated.

For the equilibrium $H_2(g) + 1/2O_2(g) \rightarrow H_2O(g)$ with $pH_2O/pH_2 = y_o$, the partial pressure of O_2 is given by

$$pO_2 = \left(\frac{y_o}{K_{eq}(T)}\right)^2 \qquad \text{(B1)}$$

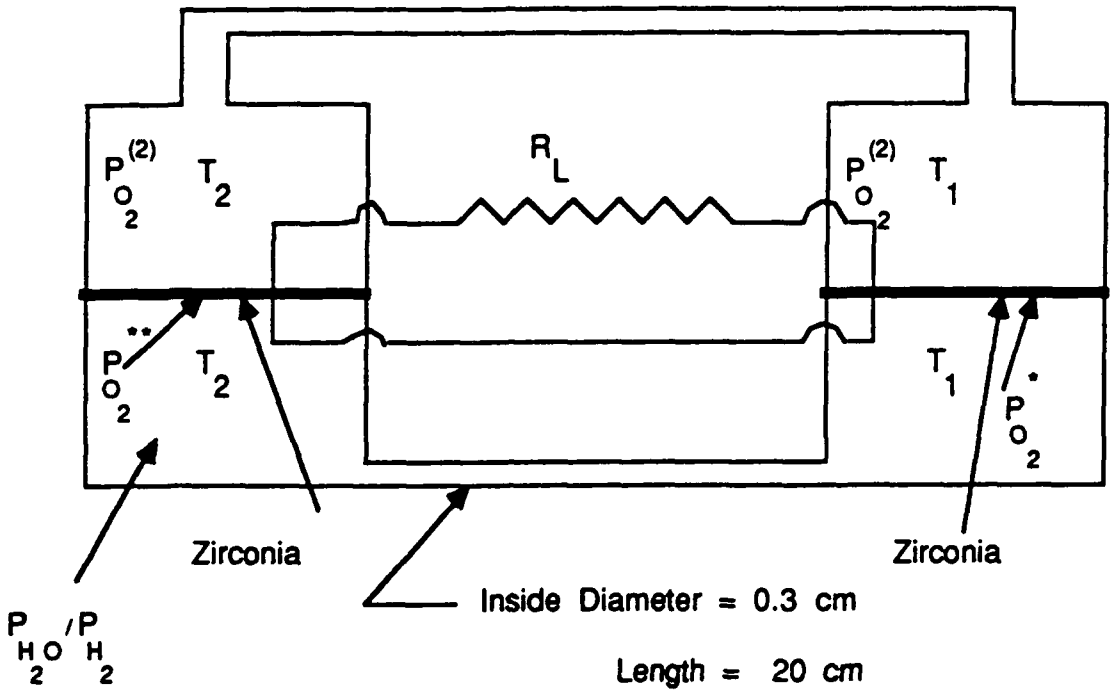

Figure #B1: A schematic showing an $O_2/H_2O/H_2$ heat engine.

for the total pressure (of $H_2 + O_2 + H_2O$) in the low pressure chamber as 1 atm. and $K_{eq}(T)$ as the equilibrium constant of the reaction $H_2(g) + 1/2O_2(g) \rightarrow H_2O(g)$. Table B gives the calculated values of pO_2 and EMF as a function of temperature for $y_o = pH_2O/pH_2 = 1.0$.

By lowering the electrolyte and the electrode resistances, substantial power densities can be realized. Electrolyte resistance may be lowered by making the electrolytes as thin as possible as well as by enhancing the the operating temperature. Using tape casting, Ceramatec routinely makes zirconia electrolytes of thickness less than 100 μm. Stabilized zirconia and thoria may be used as electrolyte materials since both of these can be operated at high temperatures and are stable in hydrogen containing atmospheres. For example, the equilibrium oxygen partial pressure for Th/ThO_2 equilibrium at 1500K is $\sim 10^{-33}$ atm. In the proposed plan of research, theoretical aspects of the modified oxygen heat engine will be invetigated. Characteristics of the heat engine will be studied experimentally. Efforts will also be directed towards the development of efficient electrode materials with low charge transfer resistance and low activation polarization. The details of the work are given in the proposed plan of research.

TABLE B

Temperature (K)	K_{eq}	pO_2	$E = -(RT/4F) \ln pO_2$ (mV)
1000	1.024×10^{10}	9.53×10^{-21}	993
1100	6.92×10^{8}	2.09×10^{-18}	965
1200	7.32×10^{7}	1.86×10^{-16}	936
1300	1.095×10^{7}	8.33×10^{-15}	908
1400	2.149×10^{6}	2.165×10^{-13}	879
1500	5.238×10^{5}	3.64×10^{-12}	851

REFERENCES

1) H.A. Harwig and A.G. Gerards, J. Solid State Chem., 26 (1978) 265.

2) R.J. Ruka, J. Weissbart, U.S. Patent Re. 28,792.

3) H.L. Chum and R.A. Osteryoung, Two volumes SERI/TR-332-416, April 1981.

4) T. Takahashi and H. Iwahara, Mat. Res. Bull.,13, (1978), 1447.

5) M.J. Verkerk, G.M.H. Van DeVelde, and A.J. Bjurggraaf, J. Phys. Chem. Solids 43, 1129-1136 (1982).

6) H. Iwahara, T. Esaka, T. Sato, and T. Takahashi, J. Solid State Chem. 39, 173 (1981).

7) T. Kudo and H. Obayashi, J. Electrochem. Soc.,122, 142 (1975).

8) H. Aria, T. Kunisaki, Y. Shimizu, and T. Seiyama, Solid State Ionics, 20, (1986).

9) T. Inoue, T. Setoguchi, K. Eguchi, and H. Aria, Solid State Ionics ,35 , (1989), 285.

ACKNOWLEDGEMENTS

This research is sponsored by SDIO/IST and managed by ONR. Dr. Jim Auborn is the contract monitor.